



## Guiding and Trapping of Electron Spin Waves in Atomic Hydrogen Gas

O. Vainio,<sup>1</sup> J. Ahokas,<sup>1</sup> S. Novotny,<sup>1</sup> S. Sheludiyakov,<sup>1</sup> D. Zvezdov,<sup>1,2</sup> K.-A. Suominen,<sup>1</sup> and S. Vasiliev<sup>1,\*</sup>

<sup>1</sup>*Department of Physics and Astronomy, University of Turku, 20014 Turku, Finland*

<sup>2</sup>*Kazan Federal University, 420008, 18 Kremlyovskaya Street, Kazan, Russia*

(Received 10 January 2012; published 3 May 2012)

We present a high magnetic field study of electron spin waves in atomic hydrogen gas compressed to high densities of  $\sim 10^{18}$  cm<sup>-3</sup> at temperatures ranging from 0.26 to 0.6 K. We observed a variety of spin wave modes caused by the identical spin rotation effect with strong dependence on the spatial profile of the polarizing magnetic field. We demonstrate confinement of these modes in regions of strong magnetic field and manipulate their spatial distribution by changing the position of the field maximum.

DOI: 10.1103/PhysRevLett.108.185304

PACS numbers: 67.63.Gh, 32.30.Dx, 32.70.Jz, 67.30.hj

Spin and magnetization oscillations are well-known phenomena in condensed matter physics. In solids wave-like spin excitations are caused by long-range dipolar or exchange interactions [1]. Quantized spin excitations (magnons) may exhibit collective quantum phenomena similar to Bose-Einstein condensate and superfluidity in quantum gases and liquid He. Observation of these effects in superfluid <sup>3</sup>He [2] and ferromagnets [3] have been extensively discussed recently. In quantum gases, where the interactions are weak and occur only during short collisional events, a different mechanism causes the excitation of spin waves: the identical spin rotation (ISR) effect [4,5]. This phenomenon results from exchange interactions, which become important once the de Broglie wavelength  $\Lambda_{\text{th}}$  exceeds the characteristic range  $a$  of the interatomic potential. Accumulated in numerous collisions, ISR leads to the propagation of spin excitations. The efficiency of ISR is determined by the parameter  $\mu \sim \Lambda_{\text{th}}/a$ , which becomes large for cold gases in the quantum gas limit. These gases are found within a range of densities  $n$  and temperatures  $T$  where  $n^{-1/3} \gg \Lambda_{\text{th}} \gg a$  so that the gas is in the quantum regime but not yet degenerate. This range is especially wide for the smallest atoms like H ( $a \approx 0.07$  nm). Experimentally the ISR effect was first observed in the nuclear spins of electron spin polarized H (H  $\downarrow$ ) [6], then in <sup>3</sup>He gas [7], and recently also in ultracold <sup>87</sup>Rb vapors [8,9]. The latter work has been performed in a small magnetic field, where the oscillations of the total electron and nuclear spin were studied. Pure electron waves were predicted for electron spins of H  $\downarrow$  [4,10] but have not been observed so far.

Spin transport in quantum gases is described by the complex diffusion equation for the transversal spin-polarization  $S_+ = S_x + iS_y$  [11], simplified for  $S_+ \ll S_z$  and  $\mu \gg 1$  to

$$i \frac{\partial S_+}{\partial t} = D_0 \frac{\varepsilon}{\mu} \nabla^2 S_+ + \gamma \delta B_0 S_+, \quad (1)$$

where  $D_0$  is the spin diffusion coefficient in unpolarized gas,  $\varepsilon = +1$  for bosons and  $-1$  for fermions,  $\gamma$  is the

gyromagnetic ratio, and  $\delta B_0$  is the deviation of magnetic field from its average value  $B_0$ . Equation (1) is similar to the Schrödinger equation for a particle with an effective mass  $M^* = -\hbar\mu/2D_0\varepsilon$  and a potential energy given by the second term on the right-hand side. The behavior of such quasiparticles in an inhomogeneous magnetic field depends on the signs of the parameters  $\mu$ ,  $\varepsilon$ , and  $\gamma$ . The sign of the spin-wave quality factor  $\mu$ , introduced above, is determined by the details of the interatomic potential. For hydrogen  $\mu < 0$ , whereas for <sup>3</sup>He  $\mu$  changes its sign from negative to positive when the temperature is lowered below  $\approx 0.5$  K [12]. The gyromagnetic ratio  $\gamma$  is important for the effect of the potential energy term in Eq. (1). Nuclear spin waves ( $\gamma_n > 0$ ) of H feel a lower potential energy in regions of smaller magnetic field, which causes a behavior similar to low-field seeking atomic species. In contrary, due to  $\gamma_e$  being negative, the electron spin waves behave as high field seekers, similarly to <sup>3</sup>He at  $T > 0.5$  K ( $\mu > 0$ ,  $\varepsilon = -1$ ). In addition, as  $\gamma_e/\gamma_n \approx -650$ , the strength of the potential energy for electron spin waves is much larger than that for nuclei. Consequently local magnetic field maxima become effective potential wells. We will show in this Letter that in analogy with real particles, ISR spin waves in H  $\downarrow$  may be spatially confined and manipulated by magnetic forces.

In our experiment H  $\downarrow$  gas is hydraulically compressed up to  $n \sim 10^{18}$  cm<sup>-3</sup>, as described in [13]. The gas is compressed in a thin-walled ( $2 \mu\text{m}$ ) 0.5 mm diam. Kapton tube (KT) below the flat mirror of a Fabry-Perot resonator (FPR), limited by the 12.5  $\mu\text{m}$ -thick Kapton film at the top and by the meniscus of superfluid helium at the bottom (see Fig. 1). The height  $L$  of the sample volume (SV) can be varied from 6.5 to 0.5 mm. The lifetime of the compressed sample was limited by the three-body recombination to 300–1000 s depending on the strength of the compression and starting density. The Kapton tube and the Kapton film are glued together by Stycast 1266 with the help of an epoxy disk of conical cross section. The thickness of the disk at the tube wall is  $\approx 0.5$  mm. Below the epoxy disk the outer surface of the KT is flushed with

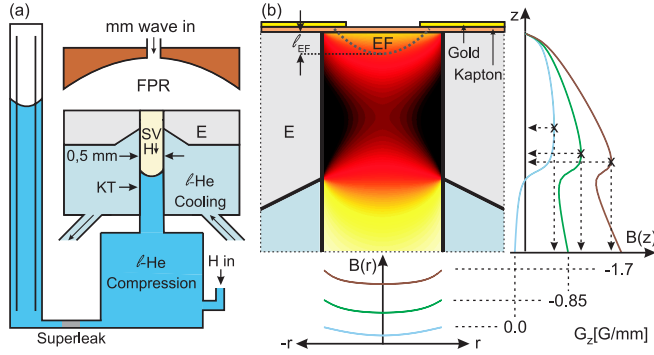


FIG. 1 (color online). (a) Schematic drawing of the sample cell showing the SV, KT, liquid-helium volumes (l-He), FPR, and epoxy structures (E). (b) Magnetic field inhomogeneity due to magnetized epoxy. The field amplitude in the top of SV is shown as a color map, dark red (dark) corresponding to the strongest and yellow (light) to the weakest field. Axial ( $z$ ) and radial ( $r$ ) cuts of the field profile through the field maximum are also shown for three different additional linear gradient values:  $-1.7$  (red/dark),  $-0.85$  (green/intermediate), and  $0$  (blue/light) G/mm.

superfluid helium that is cooled to  $T_s = 200\text{--}600$  mK. Active cooling of the SV sidewall strongly reduces the sample overheating, which is largest in the upper region of the SV. We estimate that the gas overheating did not exceed 10% of  $T_s$  for the data reported in this work. Such construction of the SV allows reaching high densities with linear response of the FPR to the electron spin resonance (ESR) in  $H \downarrow$ . Compressed H gas is coupled to the rf field of the resonator via an evanescent field (EF) beneath a subcritical (0.4 mm dia.) orifice in the gold layer on the top of the Kapton film. The evanescent field amplitude  $H_1(z)$  has an approximately Gaussian shape decreasing downwards, with an effective height of  $l_{EF} \approx 80 \mu\text{m}$  [14]. The homogeneity of the magnetic field in the compression region was limited by the weakly magnetized  $4\pi M \sim -0.8$  G epoxy disk, creating a saddle shaped field with a maximum located near the wall [see Fig. 1(b)]. We were able to reduce the inhomogeneity to  $\approx 20$  mG over the rf field region using a set of linear and parabolic shim coils, which were also capable of generating linear axial field gradients up to  $G_z = \pm 4$  G/mm.

The  $H \downarrow$  spectra were studied by continuous wave ESR in a 4.6 T field applying a 128 GHz excitation from a highly stabilized millimeter-wave source while sweeping the static magnetic field offset  $h$  through the resonance [15]. We utilized the  $b\text{--}c$  transition, since the population of the hyperfine state  $a$  is vanishingly small due to rapid exchange recombination [16]. At small enough densities  $n \lesssim 5 \times 10^{16} \text{ cm}^{-3}$  the ESR lines were inhomogeneously broadened due to the spurious field of the epoxy ring. A small positive gradient  $G_z \approx 1$  G/mm best compensated the inhomogeneity resulting in the smallest linewidths. For  $n > 10^{17} \text{ cm}^{-3}$  we observed two distinct changes in the shape of the ESR lines: (i) the main absorption peak was

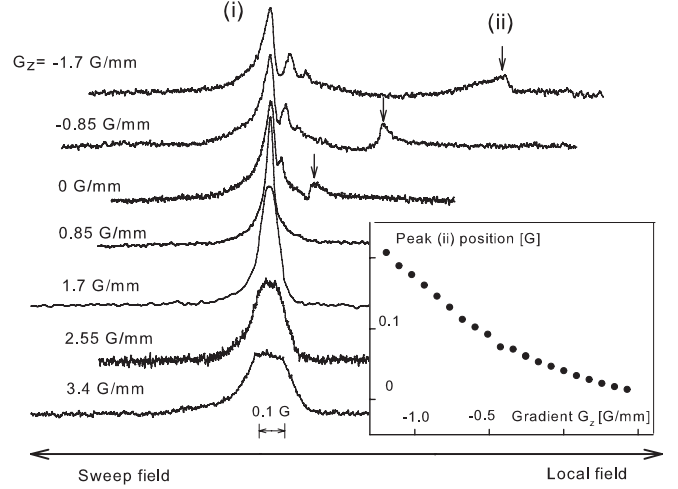


FIG. 2. ESR absorption spectra for different values of axial magnetic field gradient. The resonance frequency is fixed and magnetic field is swept through the resonance. The regions of the sample volume located in larger local fields will get in resonance at smaller sweep field. The direction of the field axis is reversed to get the local field increasing from left to right. Inset: peak (ii) position as a function of  $G_z$ .

split into several narrow lines whose position and separation depended on  $n$  and  $G_z$ , and (ii) within the range of  $G_z \approx -2 \dots +0.85$  G/mm an extra peak appeared on the right side of the spectra. These features are summarized in Figs. 2 and 3. The separation of the peak (ii) from the main ESR line increased for larger negative  $G_z$ , while for positive gradients the feature merged with the main ESR peak at  $G_z \approx +0.85$  G/mm and has not been observed on either

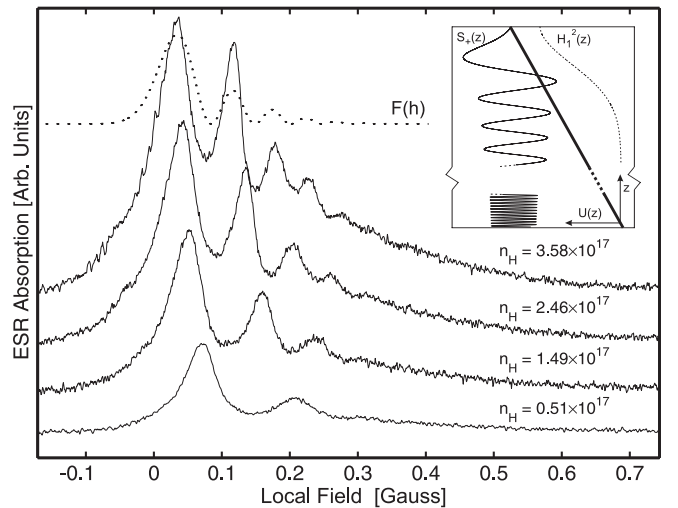


FIG. 3. ESR absorption spectra observed for samples  $G_z = -4$  G/mm. Dotted line: the simulated contribution  $F(h)$  of spin waves to the ESR absorption. In the inset the orientations of the potential  $U(z)$  (thick solid line), a spin wave mode  $S_+(z)$ , and the evanescent field  $H_1^2(z)$  are shown emphasizing the upper part of the sample volume.

side from the main resonance for larger positive gradients. The peak (ii) remained visible even at the lowest densities  $n \sim 10^{16} \text{ cm}^{-3}$  at which we were still able to resolve ESR lines. We have not observed any dependence of the peak positions of the features (i) and (ii) on the height of the gas sample, except for  $L < 0.5 \text{ mm}$ , when the sample evolved into a small bubble.

Next we consider the splitting of the main ESR peak for high densities and large negative  $G_z$  [feature (i)]. To estimate the expected separation between the ISR spin wave modes we assume an integer number of their half wavelengths between the walls of the compression region. From the ISR spin wave dispersion law  $\omega = \frac{D_0}{\mu} k^2$  we get  $\Delta\omega \lesssim \pi^2 D_0 / \mu L^2$ . Taking the minimum sample height  $L \approx 0.5 \text{ mm}$  and the values  $D_0 n = 1.5 \times 10^{18} \text{ cm}^{-1} \text{ s}^{-1}$  and  $\mu \approx 7$  from experiments with nuclear spin waves in H  $\downarrow$  [6], we find that the spin wave modes will be separated by  $\lesssim 1.5 \text{ kHz}$  at  $n = 10^{17} \text{ cm}^{-3}$ . This corresponds to  $\approx 0.5 \text{ mG}$  in the field sweep and cannot be resolved in the experiment. It is thus unlikely that the peaks seen in Figs. 2 and 3 correspond to individual spin wave modes, but rather to a number of overlapping modes. It turns out that just in the case of strong negative field deviation  $\delta H_0 = G_z z$  the overlapping modes provide a resolvable structure. The small inhomogeneity created by epoxy may be neglected in this case. A negative  $G_z$  implies that the potential shape is a box with tilted bottom decreasing downwards as  $U(z) = \gamma_e G_z z$  (inset in Fig. 3). The oscillating solutions of Eq. (1) are found in the form of Bessel functions in the radial and Airy functions in the axial direction. The shape of the solution should match the shape of the rf field excitation, which is axially symmetric and has a maximum at  $r = 0$ . Since only the zeroth-order Bessel function satisfies this condition, the solution is written as

$$S_+ \sim J_0(\kappa r) e^{i\omega t} \text{Ai}(z/\lambda + \lambda^2 k_z^2), \quad (2)$$

with  $\kappa^2 = \mu\omega/D_0$  and  $\lambda = (D_0/\gamma_e G_z \mu)^{1/3}$  being the length scale of the  $\text{Ai}(z)$  function. We apply reflective boundary conditions with zero spin flux through the walls of the cylinder. These conditions define the eigenvalues of  $\kappa$  and  $k_z$ , eigenfrequencies  $\omega$  of the oscillations, and the number of  $\text{Ai}$  function oscillations in the axial direction. For  $n = 5 \times 10^{17} \text{ cm}^{-3}$  and  $T = 260 \text{ mK}$ , we estimate  $\lambda \approx 7 \text{ }\mu\text{m}$ . In order to generate spin waves, their wave function given by Eq. (2) should overlap with the rf field. This implies that in a negative gradient we may excite only high-lying modes, which have their frequency eigenvalues in the vicinity of the intersection of the linear potential and the upper wall (see inset in Fig. 3). The total number of modes counting from the bottom of the potential  $U(z)$  and the corresponding number of  $\text{Ai}(z)$  oscillations are  $\gg L/\lambda \sim 100$  even for our shortest samples. Therefore, we deal with a quasicontinuum of mode frequencies, and excite only those with nonvanishing wave functions near

the top of the cylinder. The position of the lower boundary does not influence the shape of these modes near the top because of the rapid oscillation of  $\text{Ai}(z)$  near the bottom. This explains why the observed ESR line shapes do not depend on the sample height.

Since the position of the lower boundary does not influence the shape of  $S_+$  near the top, we consider the case of a semi-infinite cylinder. In this case the spin waves may freely propagate downwards along the slope of the magnetic potential. Sweeping the magnetic field  $h$  we scan through the region  $l_{\text{EF}}$  by tuning the rf field in resonance with electron spins. At each point the transversal magnetization is created locally and two spin waves are launched: one up and the other down. For zero axial gradient these would be similar to the electromagnetic waves in a cylindrical waveguide. Moving the point of excitation with respect to the top we scan a standing wave pattern formed by the direct and reflected waves with the spatial period equal to half wavelength. For nonzero gradients the sine waves are accelerated downwards and are replaced by the Airy functions  $\text{Ai}(z/\lambda)$ . The contribution of spin wave modes to the ESR absorption is then  $\sim F(h) = \text{Ai}^2(h/(G_z \lambda)) \times H_1^2(h/G_z)$ , shown by the dotted line in Fig. 3. This will produce maxima of absorption at the antinodes of  $\text{Ai}(z/\lambda)$ , the points  $z_i$  corresponding to the roots  $x_i$  of  $d\text{Ai}(x)/dx$ . The peak positions in the field sweep are  $h_i = G_z \lambda x_i + B_0$ . They have an  $n^{-1/3}$  density dependency since the diffusion coefficient is inversely proportional to the H density:  $nD_0 = 1.5 \times 10^{18} \text{ cm}^{-3}$  [12]. The separation between the peaks is proportional to the roots of the  $\text{Ai}$  function, which we verified as follows. First we fit the position of the leftmost peak by the relation  $h_1 = C n^{-1/3} x_1 + B_0$  with  $C$  and  $B_0$  being fitting parameters. Then we calculate the positions of the next four peaks as functions of density as  $h_i = C n^{-1/3} x_i + B_0$ . The results plotted by dashed lines in Fig. 4 match the experimental data within the error bars. The relation  $C = (G_z^2 n D_0 / \gamma_e \mu)^{1/3}$  provides the measurement of the ratio  $nD_0/\mu = 1.9(4) \times 10^{17} \text{ cm}^{-3}$ . From the fit we find  $\mu = 8(2)$ , which has been confirmed by numerical solutions of Eq. (1). The value of  $\mu$  reported here is in good agreement with the calculations of Ref. [10], and well matches that for nuclear spin waves in H  $\downarrow$  [6], as predicted by the theory [10].

The feature (ii) was best visible for zero or small negative gradients. In this case there is a local magnetic field maximum near the top of the sample and close to EF. An example of a  $\delta B(r, z)$  profile calculated for  $G_z = 0$  is presented in Fig. 1(b). Together with the wall of the tube such a field profile forms a 3D trap for the electron spin waves. A numerical solution of Eq. (1) reveals a large number of modes in this trap with the separation of a few kilohertz, again too small to be resolved. Sweeping the static field offset  $h$  we tune our excitation to resonance in different regions of the sample volume. Absorption is

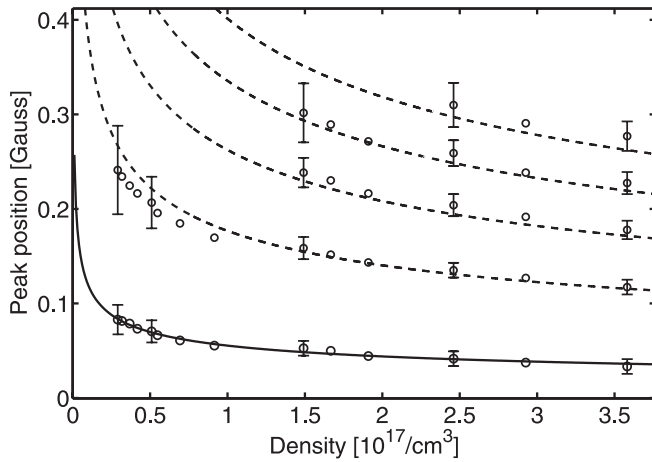


FIG. 4. Positions of spin wave peaks for samples in large negative magnetic field gradients of  $-4$  G/mm as functions of H gas density.

increased as energy is pumped into the spin wave modes and the absorption strength depends on the density of modes for a given frequency and spatial position. Applying a small linear gradient we modify the axial profile and consequently move the trap bottom up or down as shown in Fig. 1(b). The position of the corresponding spin wave peak in the ESR spectrum is determined by the static field at the trap bottom, which leads to a nonlinear dependence of the peak position on  $G_z$  (Fig. 2 inset). The spin wave modes (ii) always originate from the magnetic field maximum and therefore cannot be observed on the left from the main ESR peak, corresponding to the lower local field. For large positive gradients the field maximum is always located at the top of the cylinder, coinciding with the position of the main ESR line at the  $H_1^2(z)$  maximum. Note that if the peak (ii) would be caused by the second rf field maximum located somewhat below the main one, changing the sign of the field gradient would mirror the spectrum and this peak (ii) would be on the left-hand side with linear dependence on  $G_z$ . Remarkably, the spin wave modes (ii) are well excited and detected even by the very weak tail of the rf field. The spin wave signal is much larger than absorption due to the ESR itself. Comparing the density dependence of the two spin wave types we find that the type (ii) survive at much smaller gas densities than the propagating modes (i). These observations confirm that in case (i) we deal with a spin waveguide and with a 3D spin wave trap in case (ii).

We have also considered the possibility of magnetostatic Walker modes [17], which should exhibit a strong dependence of the mode positions on the sample geometry. However, this was not observed in our experiments. The magnetostatic modes do not depend on temperature, because they are caused by long-range dipolar forces and

do not involve atomic collisions. We verified that the separation between peaks (i) increases slightly at higher temperatures. For the ISR modes we expect a temperature dependence  $D_0/\mu \sim \sqrt{T}$  or weaker [12], which is in line with our observations. We conclude that both types of the spin wave modes described above are caused by the ISR effect.

In this work we have studied electron spin waves in atomic hydrogen quantum gas. We detected two types of spin wave excitations: travelling modes guided by the cylindrical spin waveguide and modes confined in the magnetic potential well. Similar to the matter wave interference of cold atoms [18,19], the presence of a reflective boundary in the spin waveguide leads to interference of the two travelling spin waves, one falling straight down, and the other one reflecting from the upper wall. In the quantum regime the spin waves are described as quasiparticles called magnons [2,3]. Our trapping technique resembles the original technique for trapping cold gases, but here it is realized for high field seeking quasiparticles. In further experiments we hope to observe effects of statistical correlations between trapped magnons leading to Bose-Einstein condensation and spin superfluidity.

This work was supported by the Academy of Finland (Grants No. 122595 and No. 133682) and the Wihuri Foundation. We thank D.M. Lee, N. Bigelow, G. Volovik, V. Eltsov, S. Jaakkola, J. T. M. Walraven, and L. Lehtonen for valuable discussions.

\*servas@utu.fi

- [1] A. G. Gurevich and G. A. Melkov, *Magnetization Oscillations and Waves* (CRC Press, Boca Raton, FL, 1996).
- [2] Y. M. Bunkov and G. E. Volovik, *J. Phys. Condens. Matter* **22**, 164210 (2010).
- [3] S. O. Demokritov, V. E. Demidov, O. Dzyapko, G. A. Melkov, A. A. Serga, B. Hillebrands, and A. N. Slavin, *Nature (London)* **443**, 430 (2006).
- [4] E. P. Bashkin, *JETP Lett.* **33**, No. 1, 8 (1981).
- [5] C. Lhuillier and F. Laloë, *J. Phys. (Paris)* **43**, 197 (1982).
- [6] B. R. Johnson, J. S. Denker, N. N. Bigelow, L. P. Lévy, J. H. Freed, and D. M. Lee, *Phys. Rev. Lett.* **52**, 1508 (1984).
- [7] P. J. Nacher, G. Tastevin, M. Leduc, S. B. Crampton, and F. Laloë, *J. Phys. Lett.* **45**, 441 (1984).
- [8] J. M. McGuirk, H. J. Lewandowski, D. M. Harber, T. Nikuni, J. E. Williams, and E. A. Cornell, *Phys. Rev. Lett.* **89**, 090402 (2002).
- [9] C. Deutsch, F. Ramirez-Martinez, C. Lacroûte, F. Reinhard, T. Schneider, J. N. Fuchs, F. Piéchon, F. Laloë, J. Reichel, and P. Rosenbusch, *Phys. Rev. Lett.* **105**, 020401 (2010).
- [10] J.-P. Bouchaud and C. Lhuillier, *J. Phys. (Paris)* **46**, 1781 (1985).

- 
- [11] L. P. Lévy and A. E. Ruckenstein, *Phys. Rev. Lett.* **52**, 1512 (1984).
- [12] C. Lhuillier and F. Laloë, *J. Phys. (Paris)* **44**, 1 (1983).
- [13] J. Ahokas, J. Järvinen, G. V. Shlyapnikov, and S. Vasiliev, *Phys. Rev. Lett.* **101**, 263003 (2008).
- [14] J. Järvinen, Ph.D. thesis, University of Turku (Ann. Univ. Turku. Ser. A I, No. 347, 2006).
- [15] S. Vasilyev, J. Järvinen, E. Tjukanoff, A. Kharitonov, and S. Jaakkola, *Rev. Sci. Instrum.* **75**, 94 (2004).
- [16] I. F. Silvera and J. T. M. Walraven, *Spin-Polarized Atomic Hydrogen*, edited by D. F. Brewer (North-Holland, Amsterdam, 1986), Vol. X, p. 139.
- [17] L. Walker, *Phys. Rev.* **105**, 390 (1957).
- [18] I. Bloch, T. Hänsch, and T. Esslinger, *Nature (London)* **403**, 166 (2000).
- [19] K. Härkönen, O. Vainio, and K.-A. Suominen, *Phys. Rev. A* **81**, 043638 (2010).